Simplified Expressions for Elastic Lateral Torsional Buckling of Wooden Beams

by

Arash Sahraei [a,*], Payam Pezeshky [a], Magdi Mohareb [a], and Ghasan Doudak [a]

[a] Department of Civil Engineering, University of Ottawa, Ottawa, ON, Canada K1N 6N5

Abstract

A beam finite element formulation is developed for the elastic lateral torsional buckling analysis of wood beams with rectangular cross-sections. The formulation accounts for moment gradient, load height, and pre-buckling deformation effects. The validity of the finite element and underlying variational principle is established through comparisons with critical moments obtained by 3D FEA simulations and experimental results. The validated variational expression is then adopted to develop approximate analytical expressions that separately characterize the effects of moment gradient, partial twist restraints that may exist at beam-ends, load height, and pre-buckling deformation effects. Dimensionless coefficients were formulated to characterize each effect for simple beams and cantilevers under common loading scenarios. The derived coefficients are then consolidated into a unified framework that accounts for all effects combined to predict the elastic lateral torsional buckling capacity of wooden beams.

Keywords: Lateral torsional buckling, wood beams, finite element, simplified solution, moment gradient effect, load height effect, pre-buckling deformation.

This article is to be cited as:
Sahraei A, Pezeshky P, Mohareb M, Doudak G (2018), Simplified expressions for elastic lateral torsional buckling of wooden beams, Engineering Structures, 174: 229-241.
A copy-edited version of this article can be obtained at: https://doi.org/10.1016/j.engstruct.2018.07.042

[*] Corresponding Author: Email: asahr012@uottawa.ca

Nomenclature

b	Width of cross-section
C_b	Moment gradient coefficient
C_L	Load height coefficient
C_p	Pre-buckling deformation coefficient
C_r	Partial twist coefficient
d	Cross-section depth
E	Modulus of elasticity
EL	Effective Length
G	Shear modulus
h	Cross-section height
$\mathbf{H_1}$	Vectors of the Hermitian polynomials
$\mathbf{H_2}$	Vector of Linear interpolation functions
I_{zz}, I_{yy}	Moments of inertia of the cross-section about z-axis and y-axis, respectively
J	Saint Venant torsional constant
k	Load height parameter
$\left[K_E\right]$	Elastic stiffness matrix
$\left[K_G\right]$	Geometric stiffness matrix
L	Member span
L_e	Effective length
M_a, M_b, M_c	Moments at quarter points
M_{cr}	Critical moment
M_0	Maximum bending moment
$M\left(x\right)$	Strong-axis bending moment as obtained from pre-buckling analysis
M_u	Reference elastic critical moment for the hypothetical case of a beam with simply supported ends relative to lateral displacements and twist
MGF	Moment Gradient Factor
P	Externally applied transverse point load
q_y	Distributed transverse load
R	Partial twist stiffness at beam end
u	Lateral displacement
$\left\langle u_n \right\rangle^T$	Vector of lateral nodal displacements

$\{u_s\}$	Vector of unknown displacements of the structure
U	Internal strain energy
V	Load potential energy gained
v	Transverse displacement
y_q	Height of the distributed load above section centroid
y_p	Height of a point load above section centroid
α	Twisting stiffness ratio as defined in Eq. (13)b
λ	Load multiplier
π	Total potential energy
θ_x	Angle of twist
$\langle\theta_x\rangle^T$	Vector of nodal angles of twist

1. Motivation

Elastic lateral torsional buckling (LTB) is a key failure mode that typically governs the capacity of long-span laterally unsupported wooden beams. The elastic LTB strength is known to depend on wood constitutive properties, beam geometry, load distributions, end partial fixity restraints, load height relative to section centroid, and pre-buckling deformation. The development of LTB provisions in present design standards (e.g., CAN-CSA O86-14 [1], AFPA-TR14 [2], ANSI/AWC-NDS-2015 [3]) have been primarily motivated by attaining simplified design equations. To reduce the number of parameters influencing the design, standards have adopted a number of simplifying assumptions regarding constitutive properties of wood. The resulting design equations for LTB, while simple, are restricted to a rather limited number of problems. Further, under present standard methodologies, it is unclear to the designer how to modify present design provisions to tackle deviations from material properties, boundary conditions, loading, end conditions, etc. from those postulated in formulating present design rules. Within this context, the present study aims at developing a more transparent and flexible, yet relatively simple, framework to quantify the LTB strength of laterally unsupported beams. The proposed solution incorporates key factors that affect the LTB strength of beams through independent coefficients based on approximate energy solutions.

2. Literature review

This section reviews past research on LTB of timber beams, followed by a comparative summary of LTB provisions in design standards for wooden members, and then presents an overview of theoretical lateral torsional buckling studies.

Past experimental research on the LTB of wood beams includes the work of Hooley and Madsen [4] who conducted a LTB experimental program on wooden beams with rectangular cross-sections and used them to develop design equations for elastic and inelastic LTB strength. Hindman et al. [5] experimentally investigated the LTB of unbraced cantilevers and compared test results with design standard provisions. In a subsequent study, Hindman et al. [6] expanded their work to investigate the LTB of I-joists beams. Balaz [7] investigated the LTB of timber beams with mono-symmetric cross-sections and proposed an expression to calculate the elastic critical moments. Burow et al. [8] and Burow et al. [9] provided an assessment of LTB design equations in standards by testing simply-supported and cantilevered I-joists within a wide range of slenderness ratios. Xiao et al. [10] conducted a full-scale experimental investigation on the elastic LTB of simply supported beams with rectangular cross-sections. A 3D finite element model was also developed to study the sensitivity of material properties and the effects of load height and boundary support height on the LTB capacity. Xiao et al. [11] also investigated the effect of orthotropic properties on the LTB capacity of wooden beams. Balaz and Kolekova [12] provided a generalized critical moment framework for critical moment expressions of beams with mono-symmetric cross-sections. Du et al. developed non-sway [13] and sway [14] models for LTB analysis of wooden beams. The authors also provided a comparison between results for both models [15]. Hu et al. [16] developed energy-based solutions for the LTB analysis of wooden beams with a flexible mid-span lateral brace subjected to uniformly distributed loads or mid-span point load. The same researchers also developed [17] analytical solutions and conducted a parametric study to investigate the combined effect of bracing height and load height on the elastic LTB capacity of wooden beams.

Stability behaviour of wood beam-columns have been investigated by various researchers. Among them is the study of Buchanan [18] who developed a model to predict both instability and material strength failures of lumbers under combined bending

and axial loading. Zahn [19] proposed a design criterion for wood members under combined axial and bending loads. Zahn [20] conducted an elastic buckling analysis in beam-columns to develop a general interaction equation for use in timber design. Koka [21] developed finite element solution to predict instability and material strength failures of lumber elements under combined bending and axial loading. Bell and Eggen [22] investigated the stability of beams, columns and beam-columns under combined bending and compression action using both linearized buckling and geometric nonlinear analyses. Steiger and Fontana [23] presented the results of bending-axial interaction tests performed experimentally on 220 solid rectangular specimens. Song and Lam [24], Song and Lam [25], and Song and Lam [26] performed three dimensional stability analysis for braced wood beam-columns under biaxial eccentric loading and determined lateral bracing requirements of wood beam-columns. Also, Zahn [27], Zahn [28] and Zahn [29] formulated analytically the governing equilibrium conditions for wooden rectangular beams laterally restrained along the beam centroidal axis by the shear action of deck boards.

The design guidelines for lateral torsional buckling of timber beams have been considered in standards such as CAN-CSA O86-14 [1], AFPA-TR14 [2], ANSI/AWC-NDS-2015 [3], and EN 1995-1-1: 2004 [30] where the critical moment is influenced by various parameters (e.g., moment distribution, load height, torsional flexibility at end connections, etc.). Table 1 shows the various features captured in the different standards.

Past studies on the LTB analysis for flexural members primarily focused on developing finite element formulations for wide flange steel sections. A non-exhaustive review includes the work of Krajcinovic [31] and Barsoum and Gallagher [32] who developed finite elements that capture warping effects. Shear deformation effects were included in the studies of Powel and Klingner [33], Erkmen and Mohareb [34], Attard and Kim [35], Wu and Mohareb [36], Erkmen [37], and Sahraei and Mohareb [38]. Pre-buckling deformation effects were investigated in the work Roberts and Azizian [39], Pi and Trahair [40], Andrade and Camotim [41], Machado and Cortínez [42], Erkmen and Attard [43], and Mohri et al. [44]. In a recent study, Pezeshky [45] developed a generalized lateral torsional buckling formulation that captures warping, shear deformation, pre-buckling deformation and distortion. The present solution is based on a

modification of the functional derived in Pi and Trahair [46] specifically tailored to retain features relevant to rectangular wood sections (i.e., pre-buckling deformation effects), while discarding non-important effects (e.g., warping, shear deformation, and distortion) and incorporating partial twist end-restraint effects.

Table 1 Methods used to incorporate various features in the stability design of timber beams with pin rectangular sections

Standards	Moment Distribution	Load Height	Torsional flexibility at end connections	Pre-buckling Deformation
CAN-CSA O86-14 [1]	EL*	×	Increase unsupported length by 1.15**	Not captured
AFPA-TR14 [2]	MGF***	$C_e = \sqrt{1+\eta^2} - \eta$	Increase unsupported length by 1.15	Multiply critical moment by $\gamma = 1/\sqrt{1-(b/d)^2}$
	EL	For top face loading: Increase L_e by 3d For bottom face loading: Decrease L_e by d		
ANSI/AWC-NDS-2015 [3]	EL		Increase unsupported length by 1.15	Multiply critical moment by $\gamma = 1/\sqrt{1-(b/d)^2}$
EN 1995-1-1: 2004 [30]	EL		Not captured	Not captured

*EL = Effective Length
**CAN-CSA O86-14 adopts the factor 1.15 as proposed by Hooley and Madsen [4]
***MGF = Moment Gradient Factor
b = width of section, d = depth of section, $\eta = (kd/2L_u)\sqrt{EI_{yy}/GJ}$

3. Statement of the problem

Given is a laterally unsupported prismatic wooden beam with a rectangular section subjected to general transverse loads $q(x)$ acting at a distance y_q above the centroidal axis. Under the transverse loads, the beam centroid undergoes a transverse displacement $v(x)$ from the un-deformed state (Configuration 1) to deformed Configuration 2 as shown in Fig. 1. The transverse loads are then assumed to increase to $\lambda q(x)$, where λ is a load multiplier. Under load increase, the beam is assumed to undergo a transverse displacement $\lambda v(x)$ to attain the state of onset of buckling (Configuration 3). At the

onset of buckling, the beam has tendency to undergo lateral torsional buckling characterized by lateral displacement $u(x)$ and angle of twist $\theta_x(x)$. It is required to determine the load level $\lambda q(x)$ (or critical moment λM) at the onset of buckling.

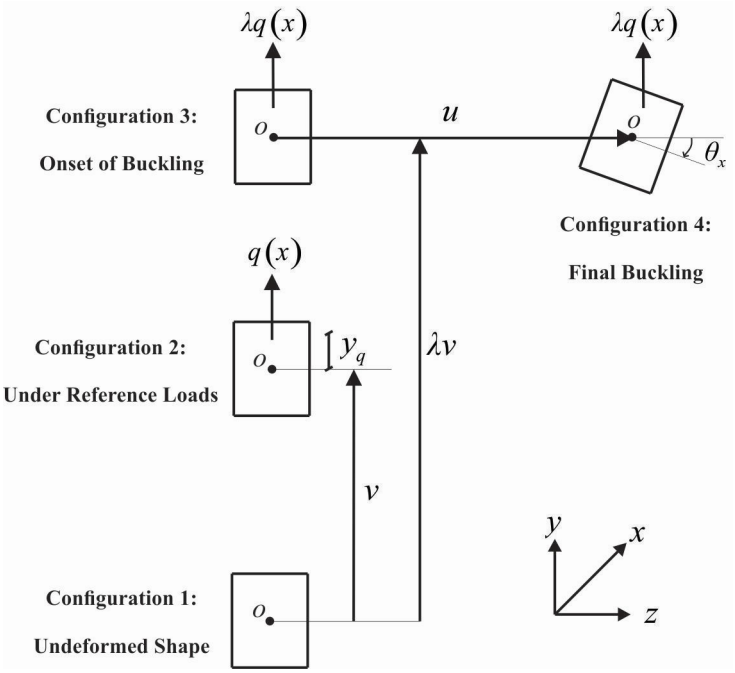

Fig. 1 Various stages of deformation

4. Assumptions

The assumptions of the solutions are:

1. The beam is prismatic with a rectangular cross-section. For rectangular sections, past studies ([16, 47, 48]) have shown that the contribution of warping is negligible on the predicted lateral torsional buckling resistance. Also, the omission of warping leads to considerable simplifications in the approximate solutions sought.
2. Wood is modelled as a homogeneous elastic orthotropic material. Given that wood properties in the tangential and radial directions are nearly identical, the nine orthotropic constants characterizing the constitutive behaviour reduce to six independent parameters. Based on 3D finite element buckling analyses, Xiao et al. [11] have shown that only two of the six constitutive properties have impact on the elastic lateral buckling capacity; (1) the longitudinal Young modulus E, and (2) the

shear modulus G for shear stresses acting on the normal plane either in the radial or tangential directions. The present formulation thus characterizes the constitutive behaviour of wood only by two independent constants E and G in a manner akin to isotropic materials.

3. The effect of pre-buckling deformations is incorporated in the solution. While most past studies have primarily focussed on I-shaped sections, and have thus omitted the effect of pre-buckling deformations, such effects have been reported to gain significance for beams with relatively shallow rectangular cross-sections ([2, 3]).
4. As transverse loads are frequently offset from the beam centroidal axis in practical situations, the solution captures the load height effect.
5. Past studies (e.g., Hooley and Madsen [4]) and design standards ([1, 2]) suggest that typical end connection details provide only partial torsional end restraints. Thus, the solution sought incorporates the effect of end partial twist restraint.
6. Given that the width to depth ratio of typical wood cross-sections is relatively large, cross-sectional distortional effects are omitted. The adoption of similar assumptions have led to solutions in excellent agreement with 3D FEA which incorporate distortional effects ([47, 48]).

5. Variational principle

Under the above assumptions, after omitting distortional, warping, and shear deformation [45] while retaining pre-buckling deformation effects, one obtains the following expression for total potential energy functional π

$$\pi \approx U_1 + U_2 + V_1 + V_2 + V_3 + V_4 \tag{1}$$

where

$$U_1 = \frac{1}{2}\int_0^L EI_{yy} u''(x)^2 \, dx$$

$$U_2 = \frac{1}{2}\int_0^L GJ\theta_x'(x)^2 \, dx$$

$$V_1 = \frac{1}{2}\int_0^L \lambda q_y(x)\, y_q(x)\, \theta_x(x)^2 \, dx \tag{2a-f}$$

$$V_2 = \int_0^L \lambda M(x) u''(x) \theta_x(x) dx$$

$$V_3 = -\int_0^L \lambda \frac{I_{yy}}{I_{zz}} M(x) u''(x) \theta_x(x) dx$$

$$V_4 = -\frac{1}{2}\int_0^L \lambda^2 \frac{\left[M(x)\right]^2}{EI_{zz}} \left(1 - \frac{I_{yy}}{I_{zz}}\right) \theta_x(x)^2 dx$$

and E is the modulus of elasticity, I_{yy} is the moment of inertia about y-axis, I_{zz} is the moment of inertia about z-axis, G is shear modulus, J is Saint-Venant torsional constant. For a rectangular section, J is computed by the expression $J \approx \left(b^3 d/3\right)\left[1 - 0.63\left(b/d\right) + 0.052\left(b/d\right)^5\right]$ (AFPA-TR14 [2]), $q_y(x)$ is the distributed load along the beam, y_q is the height of the load $q_y(x)$ from the section centroid, $M(x)$ is the bending moment distribution. Functions u and θ_x denote the lateral displacement and angle of twist respectively, and all integrals are performed over span L of the beam.

The terms U_1 and U_2 are the internal strain energies stored due to weak axis bending and Saint-Venant torsion, respectively. V_1 is the destabilizing effect due to load height effect while V_2 is the conventional destabilizing term due to strong axis bending moments. The terms U_1, U_2, V_1, and V_2 appear in conventional finite element formulation [32] while the terms V_3 and V_4 appear only when pre-buckling terms are retained in the formulation. Only when $1 - I_{yy}/I_{zz} \approx 1$, can the terms V_3 and V_4 be neglected relative to V_2. This happens to be the case for most flanged sections and hence most previous solutions do not retain these terms. However, for beams with relatively shallow rectangular cross-sections, such an approximation can underestimate the critical moments. Hence, V_3 and V_4 are retained in the present formulation.

As will be discussed under Section 8, the variational principle defined in Eqs. (1) and (2) a-f will serve as a basis for developing a series of approximate coefficients intended for design. In order to assess the accuracy of such approximate solutions, an FEA is

developed based on the variational expression in Eq. (1). The specifics of the formulation are described in the following section.

6. Finite element formulation

The lateral displacement $u(x)$ and angle of twist $\theta_x(x)$ are related to the nodal displacements and rotations $\mathbf{u_n^T} = \langle u_1 \quad u_1' \quad u_2 \quad u_2' \rangle$ and $\boldsymbol{\theta}_\mathbf{n}^\mathbf{T} = \langle \theta_{x1} \quad \theta_{x2} \rangle$ through

$$u = \mathbf{H_1^T u_n}, \qquad \theta_x = \mathbf{H_2^T \boldsymbol{\theta}_n} \tag{3a-b}$$

where

$$\mathbf{H_1^T} = \left\langle 1 - 3\left(\frac{x}{L}\right)^2 + 2\left(\frac{x}{L}\right)^3 \quad -x + \frac{2x^2}{L} - \frac{x^3}{L^2} \quad 3\left(\frac{x}{L}\right)^2 - 2\left(\frac{x}{L}\right)^3 \quad -\frac{x^3}{L^2} + \frac{x^2}{L} \right\rangle$$

is the vector of the Hermitian polynomials, and

$$\mathbf{H_2^T} = \left\langle 1 - \frac{x}{L} \quad \frac{x}{L} \right\rangle$$

is the vector of linear interpolation functions. From Eqs. (3)a-b by substituting into Eq. (1), and evoking the stationary conditions, one obtains the eigenvalue problem:

$$\left[\mathbf{K_E} - \lambda \mathbf{K_G}\right] \mathbf{u_s} = \mathbf{0} \tag{4}$$

where $\mathbf{K_E}$ is the elastic stiffness matrix, $\mathbf{K_G}$ is the geometric stiffness matrix, and $\mathbf{u_s}^\mathbf{T} = \langle \mathbf{u_n} \quad \boldsymbol{\theta}_\mathbf{n} \rangle$ is the nodal displacement vector. The above finite element solution captures the effects of load height and pre-buckling deformations and will thus serve as a benchmark to assess the approximate solutions to be developed in Section 8.

7. Verification

In a recent study, Xiao et al. [10] tested 18 specimens consisting of Spruce-Pine-Fir (SPF) No. 1/No. 2 grade lumber joists. Specimen geometries (Columns 2-4 of Table 2) were selected such that elastic lateral torsional buckling failure governs the capacity of the joists and the mechanical properties for each specimens were determined using non-destructive testing (Columns 5-7 of Table 2). All beams were simply supported at both ends and subject to a mid-span point load acting at the top face of the beam. Results based on the experimental test were compared with those based on ABAQUS 3D finite

element solution, where C3D8 brick element from the ABAQUS library was used to mesh the beams. The C3D8 element has eight nodes and three translational degrees of freedom (DOFs) per node. The experimental and numerical results in Xiao et al. [10] are thus used as benchmarks to assess the validity of the variational principle in Section 5 through comparisons with the predictions of resulting finite element formulation presented in Section 6. Excellent agreement is attained between results based on 3D FEA (Column 9) and the present FEA solution (column 10), where the ratio of the two solutions (Column 12) varied from 1.01 to 1.03 with an average of 1.01. Reasonable agreement is attained between the present finite element predictions and the experimental results where ratios varied from 0.83 to 1.31 with an average value of 1.04 and a standard deviation of 0.14 in a manner similar to the 3D FEA results. As reported in Xiao et al. [10], the difference between experimental results and FEA predictions is attributed to the spatial variability within the material and the geometric imperfections in the specimens; both effects not captured within the FEA model.

Table 2 Comparison of critical moments between test, 3D FEA, and FEA (present study) results

Spec No. (1)	Geometric Properties (mm)			Material Properties (MPa)			Critical Moment (kNm)			Ratio	
	Width (2)	Depth (3)	Span (4)	E (5)	G (6)	E/G (7)	Test (8)	3D FEA (9)	Present FEA (10)	(10)/(8) =(11)	(10)/(9) =(12)
1	38	182	4200	10434	501	21	3.34	3.21	3.25	0.97	1.01
2	38	181	4200	9022	614	15	3.72	3.33	3.38	0.91	1.02
3	38	180	4200	11185	558	20	3.58	3.47	3.52	0.98	1.01
4	38	181	4200	10111	548	18	3.62	3.31	3.34	0.92	1.01
5	39	180	4200	9947	540	18	3.62	3.49	3.53	0.98	1.01
6	38	234	3600	11217	542	21	4.60	5.05	5.08	1.10	1.01
7	38	232	3600	9745	535	18	5.67	4.68	4.71	0.83	1.01
8	38	235	3600	5563	569	10	3.44	3.80	3.86	1.12	1.02
9	38	231	3600	12339	606	20	6.30	5.52	5.57	0.88	1.01
10	38	235	3600	7619	550	14	4.87	4.30	4.35	0.89	1.01
11	39	234	3600	8092	632	13	4.78	5.13	5.20	1.09	1.01
12	38	234	3600	9009	515	17	4.51	4.46	4.49	1.00	1.01
13	38	284	4200	6668	451	15	3.16	3.77	3.83	1.21	1.02
14	38	285	4200	7171	521	14	3.28	4.24	4.30	1.31	1.01
15	39	286	4200	6469	479	14	3.68	4.18	4.25	1.15	1.02
16	38	285	4200	5960	515	12	3.87	3.85	3.94	1.02	1.02
17	38	281	4200	7880	442	18	3.19	3.99	4.03	1.26	1.01
18	38	284	4200	5491	720	8	4.53	4.42	4.56	1.01	1.03
									Minimum=	0.83	1.01
									Maximum=	1.31	1.03
									Average=	1.04	1.01
									Standard Deviation=	0.14	0.01

8. Proposed framework for elastic critical moment expression

The present study seeks an expression that approximately characterizes the elastic critical moment M_{cr} for a wood beam of rectangular sections. The approach proposes an expression of the form

$$M_{cr} \approx C_r C_b C_L C_p M_u \tag{5}$$

where

$$M_u = \frac{\pi}{L}\sqrt{EI_{yy}GJ} \tag{6}$$

is the reference elastic critical moment for the hypothetical case of a beam of span L with lateral displacements and twist restraints at both ends subjected to uniform moments. The reference moment M_u does not account for effects such as partial twist restraint, moment gradient, load height, nor pre-buckling deformation. Such effects will be accounted for separately through the modifiers $C_r C_b C_L C_p$. Specifically, C_r is a coefficient that accounts for partial twist restraint at beam-ends, C_b is a coefficient that accounts for the non-uniform moment distribution within the unsupported span, C_L is a coefficient that accounts for load position effect above the section centroid, and C_p is a coefficient that accounts for the pre-buckling deformation effects. Starting with the variational expression defined in Section 5, the following section will develop approximate expressions for coefficients C_r, C_b, C_L, and C_p for simply supported beams and then for cantilevers.

8.1. Coefficients for simply supported beams

8.1.1. Partial twist coefficient

Consider the beam to be laterally restrained but partially restrained against twist through two rotational springs with the constant stiffness R at both ends. The beam is subjected to transverse loads acting at the section centroid (i.e., $V_1 = 0$). Under the applied loads, the bending moment distribution is assumed to be $M(x)$. It is required to formulate an expression for a coefficient C_r that accounts for partial twist restraint while discarding

the effects of pre-buckling deformations, i.e., $V_3 \approx V_4 \approx 0$. Starting with Eq. (1), while adding the internal strain energy stored in the end rotational springs $R/2\left[\theta_x(0)\right]^2 + R/2\left[\theta_x(L)\right]^2$, the total potential energy π takes the form of

$$\pi = \frac{1}{2}\int_0^L EI_{yy}u''(x)^2\,dx + \frac{1}{2}\int_0^L GJ\theta_x'(x)^2\,dx + \frac{R}{2}\left[\theta_x(0)\right]^2 + \frac{R}{2}\left[\theta_x(L)\right]^2 + \int_0^L M(x)u''(x)\theta_x(x)\,dx \tag{7}$$

For loading that is symmetric relative to the mid-span point, the lateral displacement $u(x)$ and angle of twist $\theta_x(x)$ are postulated to take the form

$$u(x) = A\sin\left(\frac{\pi x}{L}\right) \qquad \theta_x(x) = B + C\sin\left(\frac{\pi x}{L}\right) \tag{8a-b}$$

Equations (8)a-b meet the boundary conditions of the problem. The presence of the constant B in Eq. (8)b stems from non-zero twist at both ends. From Eqs. (8)a-b by substituting into Eq. (7), and by evoking the stationary conditions $\partial\pi/\partial A = \partial\pi/\partial B = 0$ and $\partial\pi/\partial C$ to obtain the neutral stability condition, one has

$$\begin{bmatrix} \frac{\pi^4 EI_{yy}}{2L^3} & -\frac{M_0 I_1}{L} & -\frac{M_0 I_2}{L} \\ -\frac{M_0 I_1}{L} & 2R & 0 \\ -\frac{M_0 I_2}{L} & 0 & \frac{\pi^2 GJ}{2L} \end{bmatrix} \begin{Bmatrix} A \\ B \\ C \end{Bmatrix} = \begin{Bmatrix} 0 \\ 0 \\ 0 \end{Bmatrix} \tag{9}$$

where

$$I_1 = L\int_0^L \frac{M(x)}{M_0}\left[\left(\frac{\pi}{L}\right)^2 \sin\left(\frac{\pi x}{L}\right)\right]dx, \qquad I_2 = L\int_0^L \frac{M(x)}{M_0}\left[\left(\frac{\pi}{L}\right)^2 \sin^2\left(\frac{\pi x}{L}\right)\right]dx \tag{10a-b}$$

and M_0 is the maximum bending moment within the beam. Setting the determinant of the coefficients in Eq. (9) to zero, one recover the following expression for the critical moment

$$M_{cr} = \overline{C}_b C_r M_u = \overline{C}_b C_r \frac{\pi}{L}\sqrt{EI_{yy}GJ} \tag{11}$$

in which the expression

$$\overline{C}_b = \pi^2/2I_2 \tag{12}$$

represents an approximate moment gradient coefficient, given that the postulated displacement functions in Eqs. (8)a-b are generally approximate, and C_r is a partial twist restraint coefficient given by

$$C_r = \sqrt{\frac{1}{1+\alpha\beta_s}}, \qquad \alpha = \frac{GJ/L}{R}, \qquad \beta_s = \left(\frac{\pi I_1}{2I_2}\right)^2 \tag{13a-c}$$

Coefficient C_r characterizes the reduction in critical moment capacity due to partial twist restraint provided by end brackets. Equations (13)a-c show that C_r depends on the twisting stiffness ratio α and moment distribution through ratio β_s. The numerical values of β_s as computed by Eq. (13)c are provided in Table 3 for common loading cases. Also, given in the table is the approximate moment gradient values for $\overline{C}_b$ as computed from the expression $\overline{C}_b = \pi^2/2I_2$. As expected, by setting $R \to \infty$ into Equation (13)a-b, one obtains $C_r = 1.0$ and one recovers the critical moment expression $M_{cr0} = \left(\pi\overline{C}_b/L\right)\sqrt{EI_{yy}GJ}$ for a beam with full twist end restraint.

Table 3 Coefficients $\beta_s = \left(\pi I_1/2I_2\right)^2$ and $\overline{C}_b = \pi^2/2I_2$ for simply supported beams

Loading Case (1)	Bending moment expression $M(x)$ (2)	β_s (3)	$\overline{C}_b$ (4)	C_{b-FEA} (5)
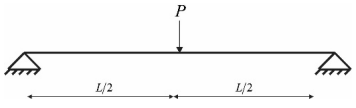	$M_1(x) = \begin{cases} 2(x/L)M_{0-Mid-PL} & 0 \le x \le L/2 \\ 2\left[1-(x/L)\right]M_{0-Mid-PL} & L/2 \le x \le L \end{cases}$	3.28	1.42	1.36
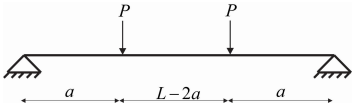	$M_2(x, a/L = 1/3) = \begin{cases} (L/a)(x/L)M_{0-2-PL} & 0 \le x \le a \\ M_{0-2-PL} & a \le x \le L-a \\ (L/a)\left[1-(x/L)\right]M_{0-2-PL} & L-a \le x \le L \end{cases}$	3.42	1.12	1.09
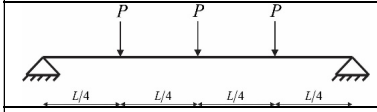	$M_3(x) = M_1(x) + M_2(x, a/L = 1/4)$	3.45	1.21	1.19
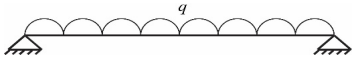	$M_4(x) = \dfrac{x(L-x)M_{0-UDL}}{(L/2)^2} \qquad 0 \le x \le L$	3.48	1.15	1.15
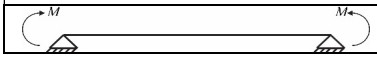	$M_5(x) = M$	4.00	1.00	1.00

In principle, both expressions for $\overline{C}_b$ and C_r are approximate since the displacement functions postulated in Eqs. (8)a-b are generally approximate. It is thus of interest to assess the effect of the approximation introduced in Eqs. (8)a-b on the results by comparing the predictions of Eq. (11) to solutions based on the present FEA. Thus, a representative reference case is considered for a simply supported beam with a 6m span and an 80mm wide x570mm deep cross-section subjected to a mid-span point load acting at the section mid-height. Material properties are $E = 12800\ MPa$ and $G = E/16$. The beam geometry is selected so that its capacity is governed by the elastic lateral torsional buckling strength according to the provisions of CAN-CSA O86-14. The critical moments are obtained from the present finite element formulated in Section 6. A mesh study has shown that eight elements are enough to attain convergence. The obtained critical moments M_{cr-FEA} are then divided by the uniform critical moment $M_u = (\pi / L)\sqrt{EI_{yy}GJ}$ to yield the moment gradient factor $C_{b-FEA} = M_{cr-FEA}/M_u$.

The numerical values for $\overline{C}_b$ in Column 4 of Table 3 slightly differ from C_{b-FEA} in Column 5. For the examined loading cases, the $\overline{C}_b/C_{b-FEA}$ ratios were found to range from 1.00 to 1.04 with an average value of 1.02. For other non-symmetric loading cases, the displacement equations postulated in Eqs. (8)a-b will lead to drastically different moment gradient predictions and a more general approach is needed to quantify the moment gradient C_b as will be discussed in subsequent sections.

Also, given the approximation introduced in Eqs. (8)a-b, it is of interest to assess the accuracy of the expression for C_r as given in Eq. (13)a, intended to capture the reduction in critical moments. Towards this goal, the reference beam previously introduced is reconsidered while replacing the full torsional end restraints with partial twist restraints of stiffness R varying from 50 kNm/rad to 200 kNm/rad. The case of full twist restraint $R \to \infty$ was found to correspond to a predicted critical moment of 105.8 kNm based on energy solution and 105.7 kNm based on FEA solution developed under section 6. For verification, a C3D8 model was built in ABAQUS (with a 150x60x4 mesh, along the span, height and width, respectively). The nine constants required to characterize the

orthotropic behaviour of Douglas-fir wood species as taken from Ádány and Schafer [49] are the longitudinal modulus of elasticity $E_L = 12{,}800\text{MPa}$; the shear moduli for stresses within the plane normal to the longitudinal direction, acting along radial and tangential directions $G_{LT} = G_{LR} = 800\text{MPa}$; and the remaining six constants $E_R/E_L = 0.05, E_T/E_L = 0.068, G_{RT}/E_L = 0.007, \nu_{LR} = 0.292, \nu_{LT} = 0.449, \nu_{RT} = 0.390$. The predicted critical moment of $M_{3D-FEA} = 103.2$ MPa is 2.4% lower than that predicted by the present finite element model. The critical moments predicted based on a modified form of Eq. (11), which replaces the approximate moment gradient $\overline{C}_b$ by the more accurate C_{b-FEA}, are compared to those based on the finite element solutions. Results in Table 4 show an excellent agreement between the prediction of Eq. (13)a for C_r and those based on the FEA solution where the ratios of both solutions (Column 6) ranges from 0.98 to 1.00, i.e., the expression for C_r given in Eq. (13)a accurately characterizes the partial twist restraint at beam ends (Table 4).

Table 4 Effect of flexible twist end restraints on elastic critical moment of 80mmx570mm glulam beam (span =6m) under mid-span point load*

Stiffness of twist end restraint $R(kNm/rad)$ (1)	Present Solution			Ratio	
	α (2)	C_r (3)	$M_{prop} = C_r C_{b-FEA} M_u$ (4)	M_{FEA} (5)	M_{prop}/M_{FEA} (6)
infinity	0.0	1.000	105.8	105.7	1.00
200	0.0591	0.915	96.8	97.6	0.99
175	0.0676	0.905	95.8	96.6	0.99
150	0.0788	0.891	94.3	95.2	0.99
125	0.0946	0.874	92.5	93.5	0.99
100	0.118	0.849	89.8	91.0	0.99
75	0.158	0.812	85.9	87.3	0.98
50	0.237	0.750	79.4	81.0	0.98
				Average=	0.99
				Standard deviation=	0.006

* $C_b = C_{b-FEA} = 1.36$ and $M_u = 77.8kNm$

8.1.2. Partial twist coefficient for different twist end restraints

As the solutions in the previous section are limited to cases where the end twisting stiffness are equal, the present section extends the work to cases where end twist stiffness

are different $R(0) = R_1 \neq R(L) = R_2$. The simply supported beam under a mid-span point load in the previous section is revisited while assuming different values for coefficients $\alpha_1 = GJ/R_1L$ and $\alpha_2 = GJ/R_2L$. The critical moments are computed from the FEA and a partial twist coefficient C_{r-FEA} (column 6 in Table 5) is obtained by dividing the critical moment by that of a beam with full twist restraint at both ends. The coefficients $C_{r1} = 1/\sqrt{1+\beta_s\alpha_1}$ and $C_{r2} = 1/\sqrt{1+\beta_s\alpha_2}$ are tabulated in Columns 3-4 of Table 5 while Column (5) provides the average values $\overline{C}_r = 0.5(C_{r1} + C_{r2})$. Column (7) provides the percentage difference $\left(\overline{C}_r - C_{r-FEA}\right)/C_{r-FEA}$. Close agreement between both solutions is observed as the percentage difference ranges from -0.2% to 0.6% with an average value of 0.1%, suggesting that adopting an average partial twist restraint $\overline{C}_r = 0.5(C_{r1} + C_{r2})$ leads to very good predictions.

Table 5 Simply supported beam under mid-span point load with different partial twist restraints at both ends

GJ/R_1L (1)	GJ/R_2L (2)	C_{r1} (3)	C_{r2} (4)	$\bar{C}_r$ (5)=[(3)+(4)]/2	C_{r-FEA} (6)	$\%diff$ (7)=[(5)-(6)]/(6)
0.000	0.059	1.00	0.921	0.960	0.962	-0.2%
0.000	0.068	1.00	0.910	0.955	0.953	0.2%
0.000	0.079	1.00	0.898	0.949	0.943	0.6%
0.000	0.095	1.00	0.882	0.941	0.939	0.2%
0.000	0.118	1.00	0.858	0.929	0.926	0.3%
0.000	0.158	1.00	0.824	0.912	0.908	0.4%
0.000	0.236	1.00	0.764	0.882	0.878	0.5%
0.059	0.068	0.921	0.910	0.916	0.916	0.0%
0.059	0.079	0.921	0.898	0.909	0.909	0.0%
0.059	0.095	0.921	0.882	0.901	0.901	0.0%
0.059	0.118	0.921	0.858	0.890	0.890	0.0%
0.059	0.158	0.921	0.824	0.872	0.872	0.0%
0.059	0.236	0.921	0.764	0.843	0.843	0.0%
0.068	0.079	0.910	0.898	0.904	0.905	-0.1%
0.068	0.095	0.910	0.882	0.896	0.896	0.0%
0.068	0.118	0.910	0.858	0.884	0.885	-0.1%
0.068	0.158	0.910	0.824	0.867	0.867	0.0%
0.068	0.236	0.910	0.764	0.837	0.837	0.0%
0.079	0.095	0.898	0.882	0.890	0.891	-0.1%
0.079	0.118	0.898	0.858	0.878	0.878	0.0%
0.079	0.158	0.898	0.824	0.861	0.860	0.1%
0.079	0.236	0.898	0.764	0.831	0.831	0.0%
0.095	0.118	0.882	0.858	0.870	0.870	0.0%
0.095	0.158	0.882	0.824	0.853	0.853	0.0%
0.095	0.236	0.882	0.764	0.823	0.823	0.0%
0.118	0.158	0.858	0.824	0.841	0.842	-0.1%
0.118	0.236	0.858	0.764	0.811	0.811	0.0%
0.158	0.236	0.824	0.764	0.794	0.794	0.0%
					MAX=	0.6%
					MIN=	-0.2%
					AVG=	0.1%

8.1.3. Moment gradient coefficient

Design standards for timber and steel members adopt one of two approaches to account for the moment gradient effects; (1) the effective length approach which have been adopted in ANSI/AWC-NDS-2015 [3], CAN-CSA O86-14 [1], and EN 1995-1-1: 2004 [30], and (2) the moment gradient approach have been used in CAN-CSA S16-14 [50], ANSI/AISC 360-16 [51], and AS-4100 [52]. For members with rectangular sections warping effects tend to be negligible, and both approaches become equivalent, while for other types of cross-sections (e.g., I-shaped), the moment gradient approach provides more consistent results [53]. Various standards have proposed different expressions for

moment gradient factors for beam segments with lateral and torsional supports at both ends under general moment distributions. For example, the AFPA-TR14 [2] proposes the expression $C_{b-AFPA} = 12.5M_{\max} / 3M_a + 4M_b + 3M_c + 2.5M_{\max}$, the CAN-CSA S16-14 [50] proposes the expression $C_{b-CAN} = 4M_{\max} / \sqrt{M_{\max}^2 + 4M_a^2 + 3M_b^2 + 4M_c^2}$, while the Australian standards AS-4100 [52] proposes $C_{b-AUS} = 1.7M_{\max} / \sqrt{M_a^2 + M_b^2 + M_c^2}$, where M_a = moment at quarter span, M_b = moment at mid-span, M_c = moment at three quarter span, and $M_{\max}$ = peak moment within the span. The Eurocode Guide does not provide a unified moment gradient equation, but instead gives load-specific moment gradient values C_{b-EUR} for a number of practical cases (Tables 6.10 and 6.11 in Gardner and Nethercot [54]). The moment gradients based on the above four standards are provided in Table 6 for common loading cases; Uniformly Distributed Load (UDL), Mid-span Point Load (Mid-PL), 2 Point Loads (2-PL) at quarter and third-quarter points, and linear bending moments where the end moment ratio ψ (Fig. 2) varies from $\psi = +1$ to $\psi = -1$. To assess the accuracy of the various Moment Gradient Factor (MGF) equations, a comparison with moment gradients predicted by the finite element analysis is provided. The critical moment M_{cr-FEA} obtained for a simply supported beam with an 8m span and 80mmx570mm cross-section is provided in Table 6 and the corresponding moment gradient as calculated from $C_{b-FEA} = M_{cr-FEA} / M_u$. When obtaining M_{cr-FEA}, the pre-buckling deformation and load height effects have been omitted by discarding the terms V_1, V_3, V_4 from the functional in Eq. (1).

As observed, the best agreement with FEA predictions is obtained for the Australian Steel Standards where the moment gradient ratio lies between 0.94 and 1.08, with an average difference of 0.99. The comparison suggests the adoption of the AS-4100 moment gradient expression $C_{b-AUS} = 1.7M_{\max} / \sqrt{M_a^2 + M_b^2 + M_c^2}$ given its accuracy and simplicity (as it involves three sampling points compared to four sampling points in other MFG equations).

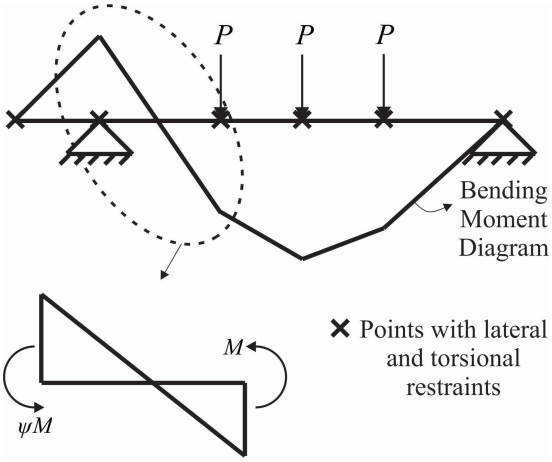

Fig. 2 Bending moment diagram and definition of end moment ratio ψ

Table 6 Summarized MGF for an 80mmx570mm rectangular section of 8m span under various loading cases

Bending moment pattern	Moment Gradient Factors					Moment gradient factor/FEA			
	FEA (1)	Eurocode Guide (steel) MFG (2)	AFPA Equation (3)	Australian Steel Code Equation (4)	Canadian Steel Code Equation (5)	(6)= (1)/(2)	(7)= (1)/(3)	(8)= (1)/(4)	(9)= (1)/(5)
$\psi = 1$	1.00	1.00	1.00	1.00	1.00	1.00	1.00	1.00	1.00
$\psi = 0.75$	1.15	1.14	1.11	1.12	1.13	1.01	1.04	1.03	1.02
$\psi = 0.5$	1.32	1.32	1.25	1.30	1.29	1.00	1.06	1.02	1.02
$\psi = 0.25$	1.53	1.56	1.43	1.53	1.50	0.98	1.07	1.00	1.02
$\psi = 0$	1.78	1.88	1.67	1.82	1.75	0.95	1.07	0.98	1.02
$\psi = -0.25$	2.07	2.28	2.00	2.16	2.03	0.91	1.04	0.96	1.02
$\psi = -0.5$	2.36	2.70	2.17	2.48	2.29	0.87	1.09	0.95	1.03
$\psi = -0.75$	2.62	2.93	2.22	2.59	2.41	0.89	1.18	1.01	1.09
$\psi = -1$	2.59	2.75	2.27	2.40	2.31	0.94	1.14	1.08	1.12
UDL	1.15	1.13	1.14	1.17	1.13	1.02	1.01	0.98	1.02
Mid-PL	1.36	1.37	1.32	1.39	1.27	0.99	1.03	0.98	1.07
2-PL	1.10	1.05	1.14	1.17	1.13	1.05	0.96	0.94	0.97
					Average=	0.97	1.06	0.99	1.03
					Standard Deviation=	0.06	0.06	0.04	0.04

8.1.4. Load height coefficient

Consider a simply supported beam laterally and torsionally restrained at both ends. The beam is subjected to a UDL q acting at a distance y_q above the centroid, and a series of $i = 1, 2, ...n_p$ equidistant point loads of equal magnitude P located at distances x_i from the left support, and acting at a height y_p above the section centroid. The bending moment $M(x)$ corresponding to the superposition of the UDL q and the point loads P has a peak value M_0. It is required to formulate an expression for a coefficient C_L that accounts for load height effect while neglecting the effects of pre-buckling deformations. The total potential energy in Eq. (1), while retaining the internal strain energy terms U_1, U_2, the destabilizing terms V_1 due to bending moments, and V_2 due to load height, and omitting the terms related to pre-buckling deformations ($V_3 \approx V_4 \approx 0$), takes the form of

$$\pi = \frac{1}{2}\int_0^L EI_{yy}u''(x)^2\,dx + \frac{1}{2}\int_0^L GJ\theta_x'(x)^2\,dx + \int_0^L M(x)u''(x)\theta_x(x)\,dx + \frac{1}{2}q\int_0^L y_q\theta_x(x)^2\,dx + \frac{1}{2}Py_p\sum_{i=1}^{n_p}\theta_{xi}(x)^2 \tag{14}$$

where the last term of Eq. (14), incorporates the additional destabilizing effect due to the point load being offset from the section centroid. The lateral displacement $u(x)$ and the angle of twist $\theta_x(x)$ are postulated to take the form

$$u(x) = A\sin\left(\frac{\pi x}{L}\right), \qquad \theta_x(x) = B\sin\left(\frac{\pi x}{L}\right) \tag{15}a\text{-}b$$

From Eqs. (15)a-b, by substituting into Eq. (14) and evoking the stationary conditions $\partial\pi/\partial A = \partial\pi/\partial B = 0$, the following conditions of neutral stability can be written:

$$\begin{bmatrix} \frac{\pi^4 EI_{yy}}{2L^3} & \frac{-M_0 I_2}{L} \\ \frac{-M_0 I_2}{L} & \frac{\pi^2 GJ}{2L} - \frac{L}{2}qy_q - Py_p\sum_{i=1}^{n_p}\left[\sin\left(\frac{\pi x_i}{L}\right)\right]^2 \end{bmatrix}\begin{Bmatrix} A \\ B \end{Bmatrix} = \begin{Bmatrix} 0 \\ 0 \end{Bmatrix} \tag{16}$$

where it is recalled that M_0 is the maximum bending moment and I_2 has been defined in Eq. (10)b. In terms of moment gradient factor, it can also be expressed as

$$I_2 = \pi^2 / 2C_b \tag{17}$$

In Eq. (16), Point loads P and UDL q need to be expressed in terms of the peak bending moment M_0, as given in Table 7 for common loading case. By setting the determinant of the coefficient matrix in Eq. (16) to zero, one obtains the critical moment as

$$M_{cr} = \frac{EI_{yy}\pi^3}{4I_2^2 L}\left\{\sqrt{\left[4\frac{GJ}{EI_{yy}}I_2^2 + \left[\varphi(M_0)\right]^2\right]} - \varphi(M_0)\right\} \tag{18}$$

where

$$\varphi(M_0) = \pi\left\{\frac{Py_p}{M_0}\left[\sum_{i=1}^{n_p}\sin^2\left(\frac{\pi x_i}{L}\right)\right] + \frac{qLy_q}{2M_0}\right\} \tag{19}$$

For the special case where all loads are applied at the section centroidal axis, $\varphi(M_0) = 0$, and Eq. (18) reverts to the critical moment expression

$$M_{cr0} = \left(\pi^3 / 2I_2 L\right)\sqrt{EI_{yy}GJ} \tag{20}$$

By dividing Eq. (18) by M_{cr0}, one obtains the sought load height coefficient

$$C_L = \frac{M_{cr}}{M_{cr0}} = \sqrt{1+\eta^2} - \eta \tag{21}$$

where $\eta = \left[\varphi(M_0)/2I_2\right]\sqrt{EI_{yy}/GJ}$. From Eq. (19), by substituting $\varphi(M_0)$ into the expression for η, one obtains

$$\eta = \frac{\pi}{2I_2}\left\{\frac{Py_p}{M_0}\left[\sum_{i=1}^{n_p}\sin^2\left(\frac{\pi x_i}{L}\right)\right] + \frac{qLy_q}{2M_0}\right\}\sqrt{\frac{EI_{yy}}{GJ}} \tag{22}$$

For the special case of uniformly distributed load applied at a height y_q, expression (22) leads to $\eta = 1.46\left(y_q/L\right)\sqrt{EI_{yy}/GJ}$. When the load is applied at the top face $y_q = h/2$, η takes the form $\eta = 1.46\left(h/2L\right)\sqrt{EI_{yy}/GJ}$, which compares to $\eta = \left(k_{AFPA}h/2L\right)\sqrt{EI_{yy}/GJ} = 1.44\left(h/2L\right)\sqrt{EI_{yy}/GJ}$ reported in AFPA-TR14. In general, for top face loading, the present solution will take the form $\eta = \left(kh/2L\right)\sqrt{EI_{yy}/GJ}$, which is similar to that reported in the AFPA $\eta = \left(k_{AFPA}h/2L\right)\sqrt{EI_{yy}/GJ}$. A comparison

between k and k_{AFPA} for other loading cases of interest is provided in Table 7. Unlike the k_{AFPA} values that are specific to certain types of loading applied at the top face, Eq. (22) provides a basis to determine k for more general loading applied at any height y_q.

Table 7 Load height parameter value k for top face loading

Loading Cases	M_0	k based on present study	k_{AFPA} based on AFPA
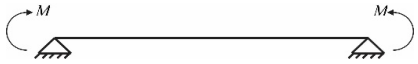	M	N/A	N/A
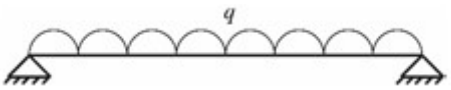	$\frac{qL^2}{8}$	1.46	1.44
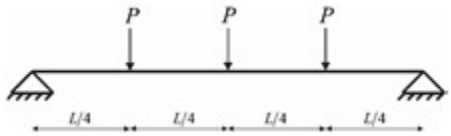	$\frac{PL}{2}$	1.54	1.45
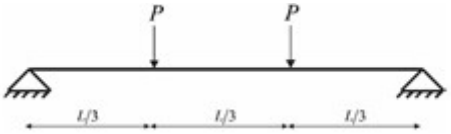	$\frac{PL}{3}$	1.60	1.63
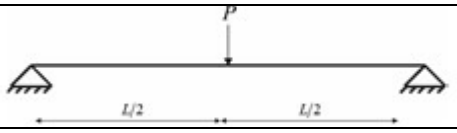	$\frac{PL}{4}$	1.81	1.72

Consider the reference beam previously defined under two loading scenarios (1) mid-span PL and (2) UDL, both applied at the beam top face. The critical moment predictions based on the expression $M_{cr} = C_b C_L M_u$ where $C_b = C_{b-FEA}$ and C_L is based on Eq. (21) are compared with FEA solutions (Table 8). Excellent agreement is attained between FEA results and the proposed equation. For the case of mid-span PL, the ratio between both predictions as provided in Column 6 ranges from 1.01 to 1.03 with an average of 1.02 and for the UDL, the ratio varies from 1.00 to 1.01 with an average of 1.00 (Column 10).

Table 8 Summary of results for interaction between moment gradient factor and load height effects

L(m) (1)	M_u *(kNm)* (2)	Mid-span PL				UDL			
		C_L (3)	$M_{cr}=C_bC_LM_u$ (4)	M_{FEA} *(kNm)* (5)	(6)= (4)/(5)	C_L (7)	$M_{cr}=C_bC_LM_u$ (8)	M_{FEA} *(kNm)* (9)	(10)= (8)/(9)
6	77.8	0.84	88.9	86.7	1.03	0.87	77.8	77.4	1.01
7	66.7	0.86	78.0	76.5	1.02	0.88	67.5	67.7	1.00
8	58.4	0.87	69.1	68.4	1.01	0.90	60.4	60.2	1.00
9	51.9	0.89	62.8	61.8	1.02	0.91	54.3	54.1	1.00
10	46.7	0.90	57.2	56.4	1.01	0.92	49.4	49.2	1.00
				Average=	1.02			Average=	1.00
				Standard Deviation=	0.008			Standard Deviation=	0.004

* $C_b = C_{b-FEA} = 1.36$ for mid-span PL and $C_b = C_{b-FEA} = 1.15$ for UDL

It is of interest to note that for mid-span loading, the moment gradient coefficient (Section 8.1.3) and load height coefficient (Section 8.1.4) yield the following expression for the critical moment

$$M_{cr} = 1.36\left\{\sqrt{1+\left(1.81y_g/k_yL\sqrt{EI_{yy}/GJ}\right)^2}-\left(1.81y_g/k_yL\sqrt{EI_{yy}/GJ}\right)\right\}\frac{\pi}{L}\sqrt{EI_{yy}GJ}$$

A nearly identical can be obtained after omitting the mono-symmetry and warping effects contributions in Balaz and Kolekova [12] where in lieu of the 1.36 factor above Balaz and Kolekova provide 1.35, and instead of the 1.81 factor, they provide1.74. Likewise, for UDL, the present solution provides the expression

$$M_{cr} = 1.15\left\{\sqrt{1+\left(1.46y_g/k_yL\sqrt{EI_{yy}/GJ}\right)^2}-\left(1.46y_g/k_yL\sqrt{EI_{yy}/GJ}\right)\right\}\frac{\pi}{L}\sqrt{EI_{yy}GJ}$$

which nearly coincides with the Balaz and Kolekova [12] expressions, where the 1.15 is replaced by 1.13 and the 1.46 is replaced by 1.44.

8.1.5. Pre-buckling coefficient

As discussed after Eq. (5), it is required to develop an expression for a coefficient C_p that characterizes the influence of pre-buckling deformation effects for a simply supported beam, both laterally and torsionally, under general loading. When developing the required expression, the loads are assumed to act at the centroidal axis, i.e., $V_1 \approx 0$, while all other terms $(U_1, U_2, V_2, V_3, V_4)$ are retained. The resulting total potential energy expression in Eq. (1) takes the form

$$\pi = \frac{1}{2}\int_0^L EI_{yy}u''(x)^2\,dx + \frac{1}{2}\int_0^L GJ\theta_x'(x)^2\,dx + \frac{1}{2}\int_0^L \left\{ 2\lambda M(x)\left(1-\frac{I_{yy}}{I_{zz}}\right)u''(x)\theta_x(x) - \lambda^2\frac{M^2(x)}{EI_{zz}}\left(1-\frac{I_{yy}}{I_{zz}}\right)\theta_x(x)^2 \right\} dx \tag{23}$$

Starting with the assumed displacement functions introduced in Eqs. (15)a-b, substituting into Eq. (23), and evoking the stationary conditions $\partial\pi/\partial A = \partial\pi/\partial B = 0$, one obtains

$$\begin{bmatrix} \dfrac{\pi^4 EI_{yy}}{2L^3} & \dfrac{-M_0}{L}\left(1-\dfrac{I_{yy}}{I_{zz}}\right)I_2 \\ \dfrac{-M_0}{L}\left(1-\dfrac{I_{yy}}{I_{zz}}\right)I_2 & \dfrac{\pi^2 GJ}{2L} - \dfrac{LM_0^2}{EI_{zz}}\left(1-\dfrac{I_{yy}}{I_{zz}}\right)\chi \end{bmatrix} \begin{Bmatrix} A \\ B \end{Bmatrix} = \begin{Bmatrix} 0 \\ 0 \end{Bmatrix} \tag{24}$$

where $\chi = (1/L)\int_0^L M(x)^2 / M_0^2\left[\sin(\pi x/L)\right]^2 dx$ and M_0 has been defined as the peak moment. Setting to zero the determinant of the matrix in Eq. (24) yields the critical moment equation

$$M_{cr} = \frac{\pi^3\sqrt{EI_{yy}GJ}}{l\sqrt{2\left(1-\dfrac{I_{yy}}{I_{zz}}\right)\left[\pi^4\dfrac{I_{yy}}{I_{zz}}\chi + 2I_2^2\left(1-\dfrac{I_{yy}}{I_{zz}}\right)\right]}} \tag{25}$$

For the special case where pre-buckling deformation effects are neglected, one has $\chi = 0$ and $\left[1-\left(I_{yy}/I_{zz}\right)\right] = 1$. In such a case, Eq. (25) reverts to the critical moment expression M_{cr0} as given by Eq. (20). Dividing Eq. (25) by M_{cr0}, one obtains the sought pre-buckling deformation coefficient C_p, which takes the form

$$C_p = \frac{M_{cr}}{M_{cr0}} = \frac{1}{\sqrt{\left(1-I_{yy}/I_{zz}\right)\left(1+\delta_s\, I_{yy}/I_{zz}\right)}} \tag{26}$$

where $\delta_s = \pi^4\chi/2I_2^2 - 1$ is a dimensionless constant that depends on the load distribution and is provided in Table 9 for common loading cases. The pre-buckling coefficient in (26) is numerically very close to the value $1/\sqrt{1-I_{yy}/I_{zz}} = 1/\sqrt{1-(b/d)^2}$ reported in Hooley and Madsen [4] and AFPA-TR14 [2]. The development of Eq. (26) is limited to the case of full twist end restraints. It is thus required to assess its applicability for the

case of partial twist restraint through comparison with FEA predictions. A 12m span beam is considered with a 215mmx570mm cross-section under uniform bending moment. Partial twist end restraints with stiffness values R varying from 50 kNm/rad to 1000 kNm/rad are considered. Table 10 provides the dimensionless twisting stiffness ratio $\alpha = GJ/LR$ and the corresponding partial twist coefficient C_r as given by Eq. (13)a. The results show that Eq. (26) slightly overestimates the critical moment for the case of partial twist restraint, as the ratio of the two solutions ranges from 1.01 at $\alpha =$ 0.96 (Column (6) of Table 10) to 1.09 at $\alpha = 1.92$ with an average value ratio of 1.03.

Table 9 Pre-buckling deformation coefficient $C_p = 1/\sqrt{\left(1 - I_{yy}/I_{zz}\right)\left(1 + \delta_s\, I_{yy}/I_{zz}\right)}$ for various loading cases

Loading Cases	δ_s
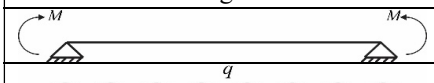	0
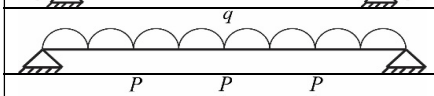	3.18×10^{-2}
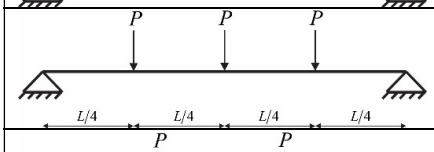	3.58×10^{-2}
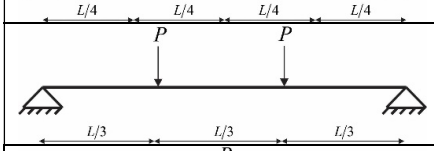	4.01×10^{-2}
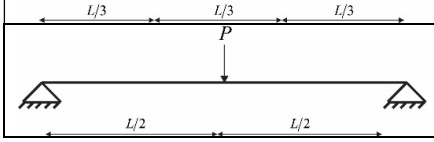	8.56×10^{-2}

Table 10 Effect of partial twist end restraints on elastic critical moment of 215mmx570mm glulam beam (span =12m)

Stiffness of end rotational restraint (1) $R(kNm/rad)$	Present Solution			FEA	$M_{present}/M_{FEA}$ (6)
	$\alpha = GJ/LR$ (2)	C_r (3)	$M_{present} = C_r C_p M_u$ (4)	M_{FEA} (5)	
50	1.92	0.339	253	232	1.09
100	0.960	0.455	340	316	1.07
200	0.480	0.585	437	415	1.05
300	0.320	0.662	494	476	1.04
400	0.240	0.714	533	518	1.03
500	0.192	0.752	561	549	1.02
600	0.160	0.781	583	572	1.02
700	0.137	0.804	600	591	1.02
800	0.120	0.822	613	606	1.01
900	0.107	0.837	625	618	1.01
1000	0.096	0.850	634	629	1.01
				Average	1.03
				Standard deviation	0.028

* $C_p = 1.08$ and $M_u = 691 kNm$

Fig. 3 shows the pre-buckling coefficient C_p as predicted by the expression $C_p = 1/\sqrt{\left(1 - I_{yy}/I_{zz}\right)\left(1 + \delta_s I_{yy}/I_{zz}\right)}$ versus I_{yy}/I_{zz} for a simply supported beam with a 570mm deep cross-section and a width b varying from 80mm to 250mm for five loading cases provided in Table 9. The solution based on the FEA solution is provided for comparison. Excellent agreement is observed between the predictions of the proposed equation for C_p and those based on the finite element formulation where the ratio of C_p based on present study as the C_p ratio based on FEA to that based on the equation varies from 0.99 to 1.00 for all loading case considered.

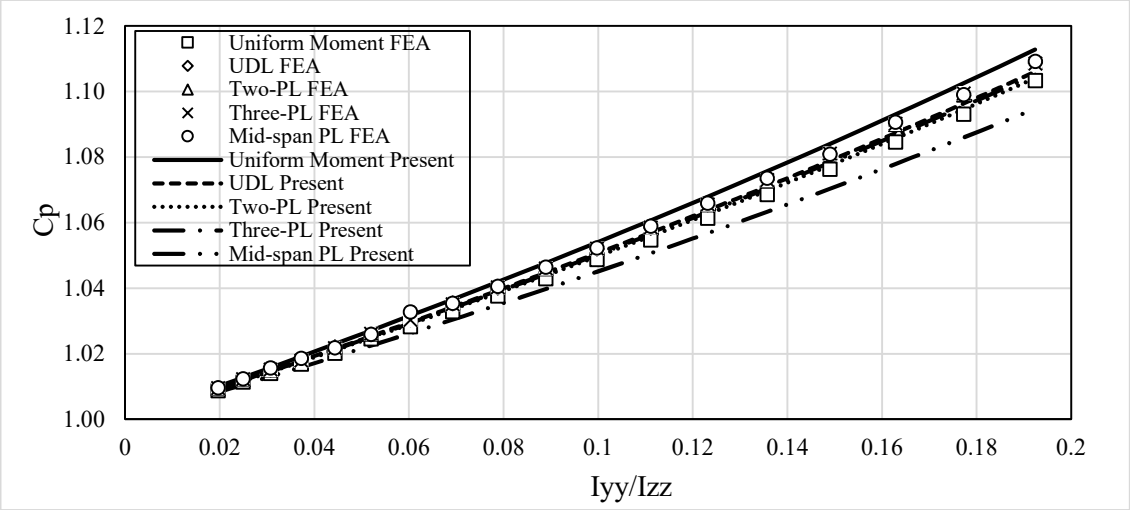

Fig. 3 Pre-buckling coefficient versus I_{yy}/I_{zz} for various loading cases

8.2. Coefficients for cantilevers

8.2.1. Moment gradient coefficient

A cantilever with an 80mmx570mm cross-section is fully fixed at the root and entirely free at the tip. Two loading cases are considered (1) a point load at the tip, and (2) a uniformly distributed load applied at section mid-height. Span is to vary from $L = 2m$ to $L = 12m$. The critical moment M_{cr-FEA} is obtained from the finite element solution and the moment gradient C_{b-FEA} is computed from the relation $M_{cr-FEA} = \left(C_{b-FEA}\pi/L\right)\sqrt{EI_{yy}GJ}$. Irrespective of the span L, the moment gradients thus computed are 1.28 for the point load and 2.05 for the uniformly distributed load cases. In comparison, in EN 1995-1-1: 2004 [30], the critical moment $M_{cr-EN} = \left(\pi/L_e\right)\sqrt{EI_{yy}GJ}$ is defined based on the effective length L_e which is given as $L_e = 0.8L$ for tip loading and $L_e = 0.5L$ for UDL. These effective lengths correspond to a moment gradient $C_b = L/L_e$ of 1.25 for point load and 2.00 for UDL, which are close to those based on the present study.

8.2.2. Partial twist coefficient

The solution provided in the previous section assumes full torsional fixity at the cantilever root, a condition that is difficult to realize in practice owing to the torsional flexibility of the connection at the root of the cantilever. In order to account for the torsional flexibility at the connection, the root of the cantilever is considered fully restrained in the lateral direction but partially restrained against twist through a partial twisting spring with stiffness of $R(0)$. For a given moment distribution $M(x)$ with a peak moment M_0, the buckling displacement fields are approximated by

$$\theta_x(x) = A + B\left[1-\cos\left(\frac{\pi x}{2L}\right)\right], \qquad u(x) = C\left[1-\cos\left(\frac{\pi x}{2L}\right)\right] \tag{27}a-b$$

By substituting into Eq. (7), setting $R(L)=0$, and evoking the neutral stability condition, one obtains $M_{cr} = C_r \bar{C}_b M_u$ where $C_r = 1/\sqrt{(1+\beta_c \alpha)}$, $\alpha = GJ/RL$, $\beta_c = 32\left(I_3/\pi\right)^2 \bar{C}_b^2$, $\bar{C}_b = \pi^2/16 I_4$, and $M_u = (\pi/L)\sqrt{EI_{yy}GJ}$. In the previous equation, the following integrals have been introduced.

$$I_3 = L\int_0^L \frac{M(x)}{M_0}\left[-\left(\frac{\pi}{2L}\right)^2 \cos\left(\frac{\pi x}{2L}\right)\right]dx,\; I_4 = L\int_0^L \frac{M(x)}{M_0}\left[\left(\frac{\pi}{2L}\right)^2 \cos\left(\frac{\pi x}{2L}\right)\right]\left[1-\cos\left(\frac{\pi x}{2L}\right)\right]dx \tag{28}a-b$$

Considering the case of point load acting at the cantilever tip, the moment distribution is $M(x) = M_0\left[1-(x/L)\right]$ which yield $I_3 = 1$, $I_4 = 0.133$, $\beta_c = 3.24\bar{C}_b^2$, and $\bar{C}_b = 4.63$. For a uniformly distributed load, the moment distribution is $M(x) = \left[(L-x)^2/L^2\right]M_0$, which yields $I_3 = 0.727$, $I_4 = 0.0655$, $\beta_c = 1.71\bar{C}_b^2$, and $\bar{C}_b = 9.41$. It is noted that the moment gradient factors $\bar{C}_b = 4.63$ and $\bar{C}_b = 9.41$ predicted by the energy solution are significantly higher than the FEA predictions in section 8.2.1. This is because the displacement functions postulated in Eqs. (27)a-b are approximate and do not satisfy the natural boundary conditions at the free end. Thus, the values of C_b will be used instead of $\bar{C}_b$ in the following steps. In contrast, the expressions for β_c and C_r provide reliable approximations for the partial twist effect in comparison to FEA predictions, provided

that they are based on coefficients C_b as obtained in Section 8.2.1 as will be shown in the following. Consider a 2m span cantilever with an 80mmx570mm cross-section, with a partial twist restraint at the root of stiffness R varying from 50-200 kNm/rad. Material properties are $E = 12800\ MPa$ and $G = E/16$. Two loading cases are considered: (1) a point load acting at the tip, and (2) a UDL. Loads are applied at the section centroid in both cases. A comparison is made between the coefficient of partial twist restraint C_r based on the equations $C_r = 1/\sqrt{(1+\beta_c\alpha)}$, $\beta_c = 3.24C_b^2$, and $C_b = C_{b-FEA} = 1.28$ to those predicted by the FEA as obtained by dividing the critical moment of a cantilever with a flexible twist end restraint of stiffness R to that of a cantilever with a rigid twist end restraint for the case of tip load (Table 11). A similar comparison for UDL is provided in (Table 12) for UDL based on $C_r = 1/\sqrt{(1+\beta_c\alpha)}$, $\beta_c = 1.71\overline{C}_b^2$, and $C_b = C_{b-FEA} = 2.05$. Excellent agreement is obtained between C_r based on FEA and the proposed equation based on energy solutions where $C_r(present)/C_r(FEA)$ ratio varies from 0.97 to 0.99 with an average of 0.98 for the case of tip point load, and varies from 1.01 to 1.05 with an average of 1.02 for UDL.

Table 11 Effect of flexible twist end restraint on elastic critical moment for 2m span Glulam cantilever with 80mmx570mm cross-section under tip point load

Stiffness of twist end restraint $R(kNm/Rad)$ (1)	Present Solution		Finite element C_{r-FEA} (4)	Ratio C_r/C_{r-FEA} (5)
	α (2)	$C_r = 1/\sqrt{(1+\beta_c\alpha)}$ (3)		
50	0.710	0.458	0.464	0.99
75	0.473	0.534	0.545	0.98
100	0.355	0.589	0.603	0.98
125	0.284	0.632	0.649	0.97
150	0.237	0.666	0.685	0.97
175	0.203	0.694	0.715	0.97
200	0.177	0.718	0.740	0.97
			Average=	0.98
			Standard deviation=	0.006

Table 12 Effect of flexible twist end restraint on elastic critical moment for 2m span Glulam cantilever with 80mmx570mm cross-section under UDL

Stiffness of twist end restraint $R(kNm/Rad)$ (1)	Present Solution		Finite element C_{r-FEA} (4)	Ratio C_r/C_{r-FEA} (5)
	α (2)	$C_r = 1/\sqrt{(1+\beta_c\alpha)}$ (3)		
50	0.710	0.306	0.405	1.05
75	0.473	0.367	0.476	1.04
100	0.355	0.414	0.530	1.03
125	0.284	0.453	0.573	1.02
150	0.237	0.487	0.608	1.02
175	0.203	0.516	0.638	1.01
200	0.177	0.541	0.663	1.01
			Average=	1.02
			Standard deviation=	0.014

8.2.3. Load height coefficient

A cantilever beam is subjected to a load $q(x)$ acting at a distance y_q above the section centroid. The following displacement functions are postulated:

$$\theta_x(x) = A\left[1-\cos\left(\frac{\pi x}{2L}\right)\right], \qquad u(x) = B\left[1-\cos\left(\frac{\pi x}{2L}\right)\right] \tag{29a-b}$$

By substituting into Eq. (14), evoking the neutral stability condition, and setting to zero the resulting matrix of coefficients while adopting a non-uniform distributed load $q(x)$ instead of the uniform load q and neglecting the last term in Eq. (14), one obtains $M_{cr} = \left[\overline{C}_b(\pi/L)\sqrt{EI_{yy}GJ}\right]\left(\sqrt{1+\eta^2}-\eta\right)$, where $\eta = (k)(y_q/L)\sqrt{EI_{yy}/GJ}$ and $k = \varsigma\pi/2I_4$, $\varsigma = L\int_0^L \left[q(x)/M_0\right]\left[1-\cos(\pi x/2L)\right]^2 dx$ which depend on the load distribution. For the case where all loads are applied at the section centroidal axis, one has $\eta = 0$, and M_{cr} reverts to the critical moment expression $M_{cro} = \overline{C}_b(\pi/L)\sqrt{EI_{yy}GJ}$ provided under section 8.2.2. By dividing M_{cr} by M_{cr0}, one recovers the sought load height coefficient C_L

$$C_L = (M_{cr}/M_{cr0}) = \left(\sqrt{1+\eta^2}-\eta\right) \tag{30}$$

For the special case of a point load P acting at the cantilever tip, one has $q(x) = P \times Dirac(L)$, $M(x) = -PL\left[1-(x/L)\right]$, $M_0 = -PL$, $k = 1.27\overline{C}_b$, and one recalls from section 8.2.2 that $\overline{C}_b = 4.63$. For the special case of a uniformly distributed load, one has $q(x) = q$, $M(x) = (q/2)(L-x)^2$, $M_0 = qL^2/2$, and $k = 1.15\overline{C}_b$, and one recalls that $\overline{C}_b = 9.41$. As discussed under Section 8.2.2, the moment gradient factors $\overline{C}_b = 4.63$ and $\overline{C}_b = 9.41$ computed from the above approximate procedure are grossly overestimated, and ought to be replaced by the moment gradients computed from FEA $C_b = C_{b-FEA}$ which take the values 1.28 and 2.05 (Section 8.2.1). An assessment of the validity of the above technique is provided through the following numerical example.

A cantilever with an 80mmx570mm cross-section and a span varying from 2-6m is subjected to two top face loading scenarios; (1) Tip point load, and (2) UDL. The critical moment predictions based on the expression $M_{cr} = C_b C_L M_u$ with $C_b = C_{b-FEA}$ and C_L is based on Eq. (30) are compared to those predicted by the FEA as obtained by dividing the critical moment of a cantilever subjected to top face loading by the critical moment subjected to centroid loading. Fig. 4 shows close agreement between the C_L expression as given by Eq. (30) and that predicted by the FEA. For the tip load, the C_L/C_{L-FEA} ratio varies from 0.96 to 1.00 with an average of 0.98. For UDL, the ratio varies from 0.97 to 1.01 with an average value of 0.98.

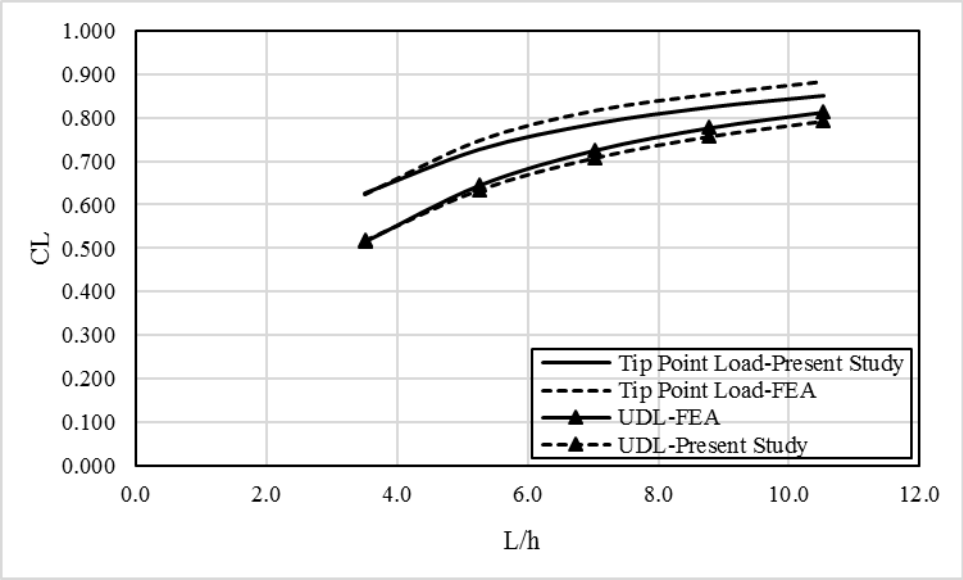

Fig. 4 Load height factor vs L/h ratio

8.2.4. Pre-buckling coefficient

Consider a cantilever under a moment distribution $M(x)$ with a peak moment M_0. By assuming the buckling displacement fields to follow those postulated in Eq. (29)a-b, substituting into Eq. (23), and evoking the neutral stability condition, one obtains $M_{cr} = \bar{C}_b M_u \Big/ \sqrt{\left[1-\left(I_{yy}/I_{zz}\right)\right]\left[1+\left(\delta_c I_{yy}/I_{zz}\right)\right]}$, where one recalls that $M_u = (\pi/L)\sqrt{EI_{yy}GJ}$, $\delta_c = -1+8\mu\bar{C}_b^2$, and $\mu = (1/L)\int_0^L \left[M(x)/M_0\right]^2\left[1-\cos(\pi x/2L)\right]^2 dx$. For the special case where one neglects the pre-buckling deformation effects, the expression for M_{cr} reverts to the critical moment expression $M_{cro} = \bar{C}_b(\pi/L)\sqrt{EI_{yy}GJ}$. By dividing M_{cr} by M_{cr0}, one obtains the sought pre-buckling coefficient

$$C_p = \left(M_{cr}/M_{cr0}\right) = 1\Big/\sqrt{\left[1-\left(I_{yy}/I_{zz}\right)\right]\left[1+\left(\delta_c I_{yy}/I_{zz}\right)\right]} \tag{31}$$

Again, as discussed under Section 8.2.2, the moment gradient factors $\bar{C}_b$ computed from the above approximate procedure are grossly overestimated, and ought to be replaced by the moment gradients computed from FEA $C_b = C_{b-FEA}$ (Section 8.2.1). Hence, using

$C_b = C_{b-FEA}$, for the special case of tip point load, δ_c in Eq. (31) takes the value $\delta_c = 0.0840$ while for the case of uniformly distributed load one has $\delta_c = 0.0253$.

Consider a cantilever with span $L = 2m$, a 570mm deep cross-section, while the section width b is assumed to vary from 80mm to 210mm. Two loading cases are considered (1) tip point load and (2) uniformly distributed loading, both acting at the section centroid. The pre-buckling coefficient as determined by the proposed technique: $C_p = \left(M_{cr}/M_{cr0}\right) = 1\Big/\sqrt{\left[1-\left(I_{yy}/I_{zz}\right)\right]\left[1+\left(\delta_c I_{yy}/I_{zz}\right)\right]}$, $\delta_c = -1+8\mu C_b^2$ are compared to those predicted by the FEA as obtained by dividing the FEA critical moment (including pre-buckling effects) by the critical moment without pre-buckling effect $C_{p-FEA} = M_{FEA}/C_b M_u$. As observed in Columns 5 and 8 of Table 13, excellent agreement is obtained between both solutions as the C_p / C_{p-FEA} ratio is found to range from 0.99 to 1.00 in all cases considered.

Table 13 Pre-buckling coefficients for a 2m cantilever

Cross-sections		Tip point load			Uniformly distributed load		
$b(mm)$ (1)	$d(mm)$ (2)	C_p (Present Study) (3)	C_{p-FEA} (4)	(5)=(3)/(4)	C_p (Present Study) (6)	C_p FEA (7)	(8)=(6)/(7)
80	570	1.01	1.01	1.00	1.01	1.01	1.00
90	570	1.01	1.01	1.00	1.01	1.01	1.00
100	570	1.01	1.01	1.00	1.01	1.01	1.00
110	570	1.02	1.02	1.00	1.02	1.02	1.00
120	570	1.02	1.02	1.00	1.02	1.02	1.00
130	570	1.02	1.02	1.00	1.03	1.03	1.00
140	570	1.03	1.03	1.00	1.03	1.03	1.00
150	570	1.03	1.03	1.00	1.03	1.03	1.00
160	570	1.04	1.04	1.00	1.04	1.04	1.00
170	570	1.04	1.04	1.00	1.05	1.04	1.00
180	570	1.05	1.05	1.00	1.05	1.05	1.00
190	570	1.05	1.06	0.99	1.06	1.06	1.00
200	570	1.06	1.06	1.00	1.06	1.06	1.00
210	570	1.06	1.07	0.99	1.07	1.07	1.00

9. Combined effects

In Section 8, the validity of each of the individual coefficients derived were established through comparisons with finite element solution. It is next of interest to assess the validity of the multiplicative expression postulated in Eq. (5). Towards this goal, the elastic critical moments are investigated for eight cases (Table 14). The problems are selected to cover different boundary conditions (either Simply Supported (SS) or Cantilever (C) in Column 2), spans (Column 3), and cross-sectional geometries (Column 4). Loading configurations included tip point loads for cantilevers, mid-span Point Load (PL) or Uniformly Distributed Load (UDL) (Column 5) and loads were applied at the section mid-height/shear centre (SC), Top Face (TF), or Bottom Face (BF) – (Column 6). Also, different levels of partial twist restraints at the ends were considered. Five cases considered pre-buckling deformation (marked as Y in Column 8) effects while the remaining three cases excluded pre-buckling effects (marked as N). In all cases, material properties were taken as $E = 12800\ MPa$ and $G = E/16$. All simply supported spans were selected such that elastic lateral torsional buckling governs the capacity according to CAN-CSA O86-14 provisions, while cantilever spans were selected in the inelastic buckling range. In both cases, the elastic critical moments were determined based on two solutions. The first one (Column 7 in Table 15) is based on the expression $M_{cr} \approx C_r C_b C_L C_p M_u$ proposed in Eq. (5), where coefficients C_r, C_b, C_L, C_p are respectively provided in Columns 2-5 of Table 15, and $M_u = (\pi/L)\sqrt{EI_{yy}GJ}$ is provided in Column 6, and the second solution (Column 8) is based on the present finite element $M_{cr}(FEA)$ and is provided for benchmarking. Close agreement between both solutions is attained in all cases as the $M_{cr}/M_{cr}(FEA)$ ratio is found to vary from 0.95 to 1.02 with a mean value of 0.98 (Column 9). For cantilevers, while inelastic LTB resistance is expected to govern the capacity (as opposed to elastic LTB), design standards such as EN 1995-1-1: 2004 [30] estimate the inelastic LTB strength from the elastic buckling stress (as calculated by dividing the elastic LTB moment M_{cr} by the elastic section modulus S_x). In this respect, the present study quantifies the elastic LTB moment M_{cr} and serves as a means to determine the required inelastic LTB strength.

Table 14 Cases investigated

Case (1)	Boundary Condition (2)	Span (m) (3)	Section Designation $b \times h$ $(mm \times mm)$ (4)	Load Type (5)	Load Position (6)	Partial Twist End Restraint (kNm/rad) (7)	Incorporate Pre-buckling Deformation Effect? (8)
1	SS	5	80x380	PL	SC	50/50	Y
2	SS	5	80x380	UDL	BF	50/100	N
3	SS	6	80x570	PL	TF	∞/∞	Y
4	SS	10	80x570	UDL	BF	1000/50	N
5	SS	8	130x646	PL	SC	∞/∞	Y
6	SS	8	130x646	UDL	TF	500/500	Y
7	C	4	130x646	PL	SC	200/0	Y
8	C	4	130x646	UDL	TF	1000/0	N

Table 15 Elastic critical moments

Case (1)	Present Study (Energy Solution)						FEA	Ratio
	C_r (2)	C_b (3)	C_L (4)	C_p (5)	$M_u\,(kNm)$ (6)	$M_{cr}\,(kNm)$ $(2)\times(3)\times(4)\times(5)\times(6)=(7)$	$M_{cr}\,(kNm)$ (8)	(7)/(8)=(9)
1	0.793	1.36	-	1.02	60.72	66.8	68.1	0.98
2	0.828	1.15	1.13	-	60.72	65.3	67.9	0.96
3	-	1.36	0.84	1.01	77.81	89.4	87.4	1.02
4	0.884	1.15	1.09	-	46.69	51.7	53.6	0.97
5	-	1.36	-	1.02	277.8	385	385	1.00
6	0.881	1.15	0.88	1.02	277.8	253	248	1.02
7	0.560	1.28	-	1.02	555.5	406	416	0.98
8	0.790	2.05	0.67	-	555.5	605	639	0.95

10. Summary and conclusions

The present study contributed to the following:

1. A total potential energy functional has been specifically tailored for the lateral torsional buckling of wood beams with rectangular sections. The formulation omits warping effects, since they are negligible for rectangular cross-sections, but accounts for pre-buckling deformation effects and partial twist restraints. The functional was then used to develop a beam finite element formulation.

2. The predictions of the present finite element are consistently within 2% of to those based on 3D FEA results. This proximity is an indication of the validity of the present finite element and the underlying variational principle. The predictions of the present

finite element (and 3D FEA models) are also in reasonable agreement with experimental results considering that the FEA does not account for the spatial variability of the mechanical properties nor the geometric imperfections in the tested specimens.

3. The validated variational expression was then used to develop approximate and relatively simple analytical expressions that characterize the effects of moment gradient, partial twist end restraints, load height, and pre-buckling deformation for common boundary conditions and loading cases.

4. The multiplicative rule proposed provides a basis to develop a generalized, transparent, and accurate framework to quantify the elastic lateral torsional buckling strength in wooden beams.

For a complete design framework, further developments are recommended to develop additional coefficients that incorporate out-of-straightness effects and resistance coefficients to incorporate the effect of material variability.

Acknowledgements

The third author gratefully acknowledges funding from the Natural Sciences and Engineering Research Council of Canada (NSERC) and additional in-kind contributions from the Canadian Wood Council (CWC).

References

[1] CAN-CSA O86-14. Engineering design in wood. CSA-O86-14 2ed. CA: CSA Group; 2017.
[2] AFPA-TR14. Designing for lateral-torsional stability in wood members. AFPA-Technical Report 14. Washington, DC, USA: American Forest & Paper Association, Inc., American Wood Council; 2003.
[3] ANSI/AWC-NDS-2015. National design specification for wood construction. ANSI/AWC-NDS-2015. Leesburg, VA, USA: American Wood Council; 2015.
[4] Hooley RF, Madsen B. Lateral Stability of Glued Laminated Beams. Journal of the Structural Division. 1964;90:201-18.
[5] Hindman DP, Manbeck HB, Janowiak JJ. Measurement and prediction of lateral torsional buckling loads of composite wood materials : Rectangular sections. Madison, WI, ETATS-UNIS: Forest Products Society; 2005b.
[6] Hindman DP, Manbeck HB, Janowiak JJ. Measurement and prediction of lateral torsional buckling loads of composite wood materials: I joist sections. 2005a;v. 55.
[7] Balaz IJ. Lateral torsional buckling of timber beams. Wood Research. 2005;50:51-8.
[8] Burow JR, Manbeck HB, Janowiak JJ. Lateral Stability Considerations for Composite Wood I-Joists. 2005.
[9] Burow JR, Manbeck HB, Janowiak JJ. Lateral Stability of Composite Wood I-Joists Under Concentrated-Load Bending. 2006;v. 49.
[10] Xiao Q, Doudak G, Mohareb M. Numerical and experimental investigation of lateral torsional buckling of wood beams. Engineering Structures. 2017;151:85-92.
[11] Xiao Q, Doudak G, Mohareb M. LATERAL TORSIONBAL BUCKLING OF WOOD BEAMS: FEA-MODELING AND SENSITIVITY ANALYSIS. World Conference on Timber Engineering. Quebec City, Canada2014.
[12] Ivan Balaz, Kolekova Y. LATERAL TORSIONAL STABILITY OF TIMBER BEAMS. 6th International Conference on Mechanics and Materials in Design. Ponta Delgada, Portugal2015.
[13] Du Y, Mohareb M, Doudak G. Nonsway Model for Lateral Torsional Buckling of Wooden Beams under Wind Uplift. Journal of Engineering Mechanics. 2016b;142:04016104.
[14] Du Y. Lateral torsional buckling of wooden beam-deck systems. Ottawa: University of Ottawa; 2016.
[15] Du Y, Mohareb M, Doudak G. LATERAL TORSIONAL BUCKLING OF TWIN-BEAM-DECK ASSEMBLIES UNDER WIND UPLIFT – SWAY VERSUS NON-SWAY MODELS. World Conference on Timber Engineering. Vienna, Austria2016a.
[16] Hu Y, Mohareb M, Doudak G. Effect of Eccentric Lateral Bracing Stiffness on Lateral Torsional Buckling Resistance of Wooden Beams. International Journal of Structural Stability and Dynamics. 2017a:1850027.
[17] Hu Y, Mohareb M, Doudak G. Lateral Torsional Buckling of Wooden Beams with Midspan Lateral Bracing Offset from Section Midheight. Journal of Engineering Mechanics. 2017b;143:04017134.
[18] Buchanan AH. Combined Bending and Axial Loading in Lumber. Journal of Structural Engineering. 1986;112:2592-609.

[19] Zahn JJ. Design of Wood Members Under Combined Load. Journal of Structural Engineering. 1986;112:2109-26.
[20] Zahn JJ. Combined-Load Stability Criterion for Wood Beam-columns. Journal of Structural Engineering. 1988;114:2612-28.
[21] Koka EN. Laterally loaded wood compression members: Finite element and reliability analysis. Vancouver: University of British Colombia; 1987.
[22] Bell K, Eggen TE. Stability of timber beams and columns. International Association for Bridge and Structural Engineering. Zurich, Switzerland: iabse symposium report; 2001. p. 30-6.
[23] Steiger R, Fontana M. Bending moment and axial force interacting on solid timber beams. Materials and Structures. 2005;38:507-13.
[24] Song X, Lam F. Three dimensional stability analysis of wood beam-columns. Proceeding 9th World Conference on Timer Engineering (WCTE). Cookeville, TN2006. p. 1061–7.
[25] Song X, Lam F. Laterally braced wood beam-columns subjected to biaxial eccentric loading. Computers & Structures. 2009;87:1058-66.
[26] Song X, Lam F. Stability Capacity and Lateral Bracing Requirements of Wood Beam-Columns. Journal of Structural Engineering. 2010;136:211-8.
[27] Zahn J. Lateral stability of deep beams with shear-beam support. Madison, WI: Forest Products Laboratory; 1965.
[28] Zahn J. Shear stiffness of two-inch wood decks for roof systems. Madison, WI: Forest Products Laboratory; 1973.
[29] Zahn JJ. Bracing Requirements for Lateral Stability. Journal of Structural Engineering. 1984;110:1786-802.
[30] 1995-1-1:2004 E. Eurocode 5: Design of Timber Structures-General - Common rules and rules for buildings. Brussels, Belgium.: European Committee of Standardization (CEN); 2004.
[31] Krajcinovic D. A consistent discrete elements technique for thinwalled assemblages. Int J of Solids and Struct. 1969;5:639-62.
[32] Barsoum RS, Gallagher RH. Finite element analysis of torsional and torsional–flexural stability problems. International Journal for Numerical Methods in Engineering. 1970;2:335-52.
[33] Powell G, Klingner R. Elastic Lateral Buckling of Steel Beams. J of the Struct Div. 1970;96:1919-32.
[34] Erkmen RE, Mohareb M. Buckling analysis of thin-walled open members—A finite element formulation. Thin Wall Struct. 2008b;46:618-36.
[35] Attard MM, Kim M-Y. Lateral buckling of beams with shear deformations – A hyperelastic formulation. Int J of Solids and Struct. 2010;47:2825-40.
[36] Wu L, Mohareb M. Buckling formulation for shear deformable thin-walled members—II. Finite element formulation. Thin Wall Struct. 2011b;49:208-22.
[37] Erkmen RE. Shear deformable hybrid finite-element formulation for buckling analysis of thin-walled members. Finite Elements in Analysis and Design. 2014;82:32-45.
[38] Sahraei A, Mohareb M. Upper and lower bound solutions for lateral-torsional buckling of doubly symmetric members. Thin Wall Struct. 2016;102:180-96.

[39] Roberts TM, Burt CA. Instability of monosymmetric I-beams and cantilevers. International Journal of Mechanical Sciences. 1985;27:313-24.
[40] Pi Y, Trahair N. Prebuckling Deflections and Lateral Buckling. II: Applications. Journal of Structural Engineering. 1992b;118:2967-85.
[41] Andrade A, Camotim D. Lateral-torsional buckling of prismatic and tapered thin-walled open Pre-buckling deflection effects on stability of thin-walled beams with open sections beams: assessing the influence of pre-buckling deflections. Journal of steel and composite structures. 2004;4:281-301.
[42] Machado SP, Cortínez VH. Lateral buckling of thin-walled composite bisymmetric beams with prebuckling and shear deformation. Engineering Structures. 2005;27:1185-96.
[43] Erkmen RE, Attard MM. Lateral–torsional buckling analysis of thin-walled beams including shear and pre-buckling deformation effects. International Journal of Mechanical Sciences. 2011;53:918-25.
[44] Mohri F, Damil N, Potier-Ferry M. Pre-buckling deflection effects on stability of thin-walled beams with open sections. Steel and Composite Structures. 2012;13:71-89.
[45] Pezeshky P. Distortional static and buckling analysis of wide flange steel beams. Ottawa, ON, CA.: University of Ottawa; 2017.
[46] Pi Y, Trahair N. Prebuckling Deflections and Lateral Buckling. I: Theory. Journal of Structural Engineering. 1992a;118:2949-66.
[47] Xiao Q, Doudak G, Mohareb M. Numerical and Experimental Investigation of Lateral Torsional Buckling of Wood Beams. Engineering Structures. 2017;Accepted.
[48] Hu Y, Mohareb M, Doudak G. Lateral Torsional Buckling of Wooden Beams with Mid-span Lateral Bracing Offset from Section Mid-height. Journal of Engineering Mechanics. 2017:Accepted.
[49] Ádány S, Schafer BW. A full modal decomposition of thin-walled, single-branched open cross-section members via the constrained finite strip method. Journal of Constructional Steel Research. 2008;64:12-29.
[50] CAN-CSA S16-14. Handbook of Steel Construction. CSA-S16-14 Specification. 10th ed. CA: Canadian Institute of Steel Construction; 2014.
[51] ANSI/AISC 360-16. ANSI/AISC 360-16. Specification for structural steel buildings. Chicago, IL: American Institute of Steel Construction (AISC); 2016.
[52] AS-4100. AS 4100 steel structures. Sydney, Australia1998.
[53] Sahraei A, Pezeshky P, Mohareb M. Lateral torsional buckling analysis and design of steel beams with continuous spans. 6th International Conference on Engineering Mechanics and Materials. Vancouver, Canada2017a. p. EMM-635.
[54] Gardner L, Nerthercot DA. Designers' Guide to Eurocode 3: Design of Steel Buildings. 2nd ed: ICE, SCI; 2011.